Energy Reports 11 (2024) 1945–1958

Contents lists available at ScienceDirect

Energy Reports

journal homepage: www.elsevier.com/locate/egyr

Research paper

Capabilities of advanced heat transfer fluids on the performance of flat plate solar collector

Gabriela Huminic *, Angel Huminic

Transilvania University of Brasov, Mechanical Engineering Department, 29, Bulevardul Eroilor, 500036 Brasov, Romania

ARTICLE INFO

Keywords:
Solar collector efficiency
Ionanofluid
Nanofluid

ABSTRACT

The main goal of the current paper is to investigate the effect of advanced heat transfer fluids including ionanofluids and nanofluids with several base fluids (ionic liquid, water and ethylene glycol) on the thermal performace of a flat-plate solar collector (FPSC). The FPSC under real weather conditions was analyzed. In the current research, the advanced heat transfer fluids investigated are: $[B_{mim}]BF_4$ (1-butyl-3-methyl imidazolium tetrafluoroborate), $[B_{mim}]BF_4$ + graphene, $[B_{mim}]BF_4$ + single-wall carbon nanotube with concentrations of 0.005 and 0.01 wt%, $[C_{4mim}]NTf_2$ (1-butyl-3-methylimidazolium bis(trifluoromethylsulfonyl)imide), $[C_{4mim}]NTf_2$ + aluminum oxide, water, water+aluminum oxide, ethylene glycol, and ethylene glycol+aluminum oxide with concentrations of 0.18, 0.36 and 0.90 vol%. FPSC efficiency is compared to existing correlations for figure-of-merits (FOMs). Results indicate that the thermal efficiency depends on the base fluid and the type of nanoparticle and varies with the nanoparticles concentration. The use of $[C_{4mim}]NTf_2$ + 0.9 vol% Al_2O_3 in FPSC led to relative enhancement in thermal efficiency by about 54.08%, 26.05% and 17.54% compared to water + 0.9 vol% Al_2O_3 at Re= 100, 200 and 300. The results also show that not all analyzed FOMs correlations are in agreement with the collector efficiency. Furthermore, the comparative study carried out emphasized that ionic liquids are a good alternative to conventional fluids (water) to be used in solar collectors under Romanian weather conditions.

1. Introduction

Romania disposes of rich and varied resources of renewable energy: solar, wind, biomass, hydro, and geothermal energies. Currently, in Romania, the thermal systems that used solar energy in buildings for hot water production, heating swimming pools and heating-cooling represent an alternative to conventional fuels. According to the renewable energy barometer, EurObserv'ER, (https://www.eurobserv-er.org/category/2021/), the installed capacity of thermal solar collectors in 2020 in Romania was 218 910 m^2 and 153.2 MWth respectively, recording an increase of 52% compared to 2010. It is estimated that by 2030, Romania will achieve the energy share from renewable sources of at least 34%, the total energy consumption from renewable sources in 2020 being 24%. The use of thermal systems such as flat-plate solar collectors (FPSC), evacuated tube solar collectors (ETC), direct absorption solar collector (DASC) or photovoltaic thermal collectors (PV/T) can contribute to achieve of this objective.

In flat-plate solar collectors (FPSCs), solar radiation is absorbed, converted it into heat and transferred to the working fluid. Since they are easy to use and have reasonably priced, the FPSCs are used for heating fluids at temperatures below 80 ℃ (Twidell and Weir 2006). Conventional working fluids used in the FPSCs are water, oil, air, and antifreeze solutions (ethylene glycol or ethylene glycol-water mixture). There are numerous methods to improve FPSCs performance such as employing different insert devices [2,3], optimizing the absorber with new configurations [4], phase change material [5], and improving working fluids properties [6–24].

In terms of improving of FPSCs performance using insert devices, García et al. (2018) conducted a comparative analysis on methods of improving heat transfer in FPSCs. For this, a solar water collector that uses insert devices (wire-coils and twisted tapes) located in Spain is considered. The experiments are done at mass flow rates per tube in the range 9–50 kg/h and fluid temperatures between 15–70 ℃. They found that the use of inserts leads to the decrease in absorber temperature and also that at higher mass flow rates (Re > 1000), all inserts shows performance comparable. FPSC performance using two heat transfer enhancers (rod and tube) is experimental investigated by Balaji et al. (2019). They noticed that for all Reynolds numbers, the efficiency of the rod heat transfer enhancer is greater than that of the tube and conventional solar collector. The FPSCs performance using a V-corrugated absorber was studied by Fan et al. (2019). They concluded the optical

* Corresponding author.
E-mail address: gabi.p@unitbv.ro (G. Huminic).

https://doi.org/10.1016/j.egyr.2024.01.044
Received 15 November 2023; Received in revised form 8 January 2024; Accepted 17 January 2024
Available online 31 January 2024

Nomenclature

A_c	collector area, $[m^2]$.
A_e	surface area of edges, $[m^2]$.
C_p	specific heat at constant pressure, $[J/kg\ K]$.
D	outer diameter of tube, $[m]$.
D_i	inner diameter of tube, $[m]$.
F	standard fin efficiency.
F'	collector efficiency factor.
F_R	removal heat factor.
G_t	solar radiation on solar collector $[W/m^2]$.
$h_{b,a}$	convection heat transfer coefficient in the bottom, $[W/m^2K]$.
$h_{e,a}$	convection heat transfer coefficient in the edges, $[W/m^2K]$.
h_{fi}	heat transfer coefficient of fluid, $[W/m^2K]$.
h_w	heat transfer coefficient of wind, $[W/m^2K]$.
k_b	thermal conductivity of insulators in the bottom, $[W/m\ K]$.
k_c	thermal conductivity of absorber plate.
k_e	thermal conductivity of insulators in the edges, $[W/m\ K]$.
k_0	incident angle modifier.
$\dot{m}$	mass flow rate, $[kg/s]$.
Mo	Mouromtseff number.
Ng	number of glass covers.
Nu	Nusselt number.
Pr	Prandtl number.
Re	Reynolds number.
Q_u	absorbed heat by plate $[W]$.
t_b	thickness of insulators in bottom, $[m]$.
t_c	thickness of absorber plate, $[m]$.
t_e	thickness of insulators in edges, $[m]$.
T_a	outside temperature, $[K]$.
$T_{f,in}$	inlet fluid temperature, $[K]$.
T_{pm}	mean temperature of plate, $[K]$.
U_b	bottom heat loss coefficient, $[W/m^2K]$.
U_e	heat loss coefficient from the collector edges, $[W/m^2K]$.
U_L	overall heat loss coefficient, $[W/m^2K]$.
U_t	top loss coefficient, $[W/m^2K]$.
v_w	wind velocity, $[m/s]$.
W	tube spacing, $[m]$.

Greek symbols

β	collector slope.
μ	viscosity, $[Pa\ s]$.
ρ	density, $[kg/m^3]$.
ε_g	infrared emissivity of glass cover.
ε_p	infrared emissivity of absorber plate.
σ	Stefan– Boltzmann constant, $[W/m^2K^4]$.
$(\tau \bullet \alpha)_e$	transmittance-absorptance product.
ϕ	nanoparticles concentration, [%].

Subscripts

bf	base fluid.
np	nanoparticle.
wf	working fluid.

and thermal efficiencies can be improved by using V-corrugated absorbers. To evaluate a FPSC using an integrated thermal energy storage unit with two different phase-change materials (PCMs), Carmona and Palacio (2019) proposed a thermal modelling strategy. Results indicated that the inclusion of PCM allows the collector's operation also at night, without significantly have an effect on the thermal performance.

In recent years, several theoretical and experimental studies were conducted to evaluate of the performance of FPSC. The studies indicated that the use of the advanced heat transfer fluids with improved thermophysical properties could improve their efficiency.

1.1. Numerical studies

Mahian et al. (2014) theoretical analyzed the potential of Cu/water, Al_2O_3/water, TiO_2/water and SiO_2/water nanofluids used in a minichannel-based solar collector, operated in Bangkok, Thailand. The research is performed at mass flow rates of 0.1 and 0.5 kg/s, a solar intensity of 830 W/m^2, the outside temperature of 308 K, and volume concentrations up to 4%. The maximum and minimum efficiency are achieved when SiO_2/water and Cu/water nanofluids are used. Moreover, the results of this analysis indicate that the efficiency is reduced with rising nanoparticles concentration. Sint et al. (2017) performed a theoretical analysis on the efficiency of FPSC using CuO-water nanofluid installed in Taunggyi, Myanmar. The experiments are carried out at different nanoparticles concentrations (0.5–3.5 vol%) and particles sizes (25–140 nm). They found that the maximum efficiency of 5% is achieved at 2.0 vol% CuO with a particle size of 25 nm. The results showed also that the nanoparticle size does not significantly influence the collector efficiency. A theoretically study of the different nanofluids used in FPSC was carried out by Liu et al. (2020). SiO_2, Al_2O_3, *GNPs*, and *Gr* added into distilled water are analyzed. The analysis was conducted for various nanoparticle concentrations (0.25–1.0 vol%), fluid inlet temperatures (30, 40, and 50 ℃), mass flow rates (0.0085, 0.017, and 0.0255 kg/s) and solar irradiance (500, 750, and 1000 W/m^2). The results showed that 1.0 vol% GNPs and 1.0 vol% Gr nanofluids enhanced the collector's efficiency up to 32.64% and 17%, while by use of 1.0 vol% SiO_2 and 1.0 vol% Al_2O_3 nanofluids in FSCS is achieved a efficiency of 4.09% and 8.26% respectively. Elcioglu et al. (2020) carried out a theoretically analysis on effectiveness of Al_2O_3/water, TiO_2/water, SiO_2/water, polystyrene/water, GNP/water, and SWCNT/water nanofluids used in a FPSC under laminar and turbulent flows, by calculating the number of Figure-of-Merits (FOMs). The thermal efficiency of FPSC using different nanofluids is compared to FOMs and they concluded that not all FOMs are applicable for to evaluate FPSC working. Ashour et al. (2022) investigated numerically the thermal performance of a FPSC using ZnO/water and CuO/ water nanofluids, located in Egypt. The test was conducted at different nanoparticles concentrations (0.05, 0.10 and 0.15 vol%) and mass flow rates (from 0.0125 to 0.025 kg/s). They found that the use of 0.15 vol% CuO/waternanofluid improves the efficiency up to 81.64% at mass flow rate of 0.0125 kg/s, while for 0.15 vol% ZnO/water nanofluid the improvement in efficiency is 77.64% at the same mass flow rate. Geovo et al. (2023) simulated the performance of FPSC using MgO/water nanofluid located in Porto Alegre, Brazil, and found that the rise of the mass flow rate rises the collector thermal efficiency, and also that the thermal efficiency rises significantly up to 1.0 vol% concentration, whereupon, the rise in thermal efficiency is less significant. Xu et al. (2022) simulate the thermal efficiency of FPSC using LS-SVR, ANFIS, MLP, CFF, GR, and RBF neural networks. Their results indicated that the LS-SVR has higher accuracy than other correlations to evaluate the thermal efficiency of the FPSC.

1.2. Experimental studies

Said et al. (2015a) investigated the thermal and exergy efficiencies of FPSC using SWCNTs/water nanofluids. The FPSC is placed to an inclination angle of 22° and tested for weather conditions in Kuala Lumpur, Malaysia. They found a maximum enhancement in thermal and exergy

efficiencies of approximately 95% and 26% at a concentration of 0.3 vol % of SWCNTs and a mass flow rate of 0.5 kg/min. In another study, Said et al. (2016) studied the impact different sizes of Al_2O_3 nanoparticles added into water on the thermal efficiency of a FPSC situated in Kuala Lumpur, Malaysia. The collector is tested in the time interval 9 a.m. - 5 p.m at an inclination angle of 22°. The experiments were carried out for two sizes of nanoparticles, 13 nmand 20 nm, three mass flow rates, 0.5, 1.0 and 1.5 kg/min, and a concentration of 0.1 vol% Al_2O_3. They concluded that the particle size does not significantly influence the collector performance. The thermal efficiency of FPSC using Al_2O_3 (13 nm)-water is 73.7%, while the efficiency of FPSC using Al_2O_3 (20 nm)-water is 70.7% at a flow rate of 1.5 kg/min. Thermal and exergetic efficiencies of the FPSC using TiO_2-water nanofluids with Polyethylene Glycol as dispersant are investigated also by Said et al. (2015b). The FPSC was tested at mass flow rates in the range 0.5–1.5 kg/min, and for 0.1 and 0.3 vol% concentrations of nanoparticles. The test conditions are similar to those in Refs. (Said et al., 2015b, 2016). The maximum thermal and exergy efficiencies of 76.6% and 16.9%, respectively were achieved for 0.1 vol% concentration and a mass flow rate of 0.5 kg/min. With increasing concentration, they found a decrease in FPSC thermal efficiency. An experimental study on the efficiency of FPSC using Cu/water nanofluids was conducted by He et al. (2015). The FPSC is located in Guangdong, China, and is fixed at a inclination angle of 45°. Two nanoparticles concentrations (0.1 and 0.2 wt%) and two particles sizes (25 and 50 nm) are considered. They affirmed that increasing both concentration and particle size does not lead to an improvement in thermal efficiency, the maximum thermal efficiency being reached for a concentration and particle size of 0.1 wt% Cu and 25 nm respectively. Sharafeldin et al. (2017) conducted an experimental research on the use of Tungsten Trioxide (WO_3)/water nanofluid in a FPSC employed in Budapest, Hungary. The FPSC was tested in sunny days between1 a.m. and 4 p.m., at mass flux rates from 0.0156 to 0.0195 kg/s•m^2 and nanoparticles concentrations of 0.0167 vol%, 0.0333 vol%, and 0.0666 vol%. They achieved an efficiency of 71.87% at a concentration of 0.0666 vol% and 0.0195 kg/s•m^2.

Verma et al. (2017) examined the effect of several nanofluids on the energetic and exergetic performance of FPSC. The tests are conducted indoors using a solar panel with 8 halogen lights of 500 W. The following nanofluids with concentrations in the range 0.25–2.0 vol% are tested: MWCNTs/water, graphene/water, CuO/water, Al_2O_3/water, TiO_2/water and SiO_2/water nanofluids. Results indicated an enhancement in thermal efficiency of 23.47%, 16.93%, 12.64%, 8.28%, 5.09% and 4.08%, respectively, for MWCNTs/water, graphene/water, CuO/-water, Al_2O_3/water, TiO_2/water and SiO_2/water nanofluids at a mass flow rate of 0.025 kg/s and a nanoparticle concentration of 0.75 vol%. For the same mass flow rate and concentration, they found an enhancement in exergetic efficiency of 21.46%, 16.67%, 10.86%, 6.97% *and*5.74% respectively for MWCNTs/water, graphene/water, CuO/-water, Al_2O_3/water, TiO_2/water and SiO_2/water nanofluids. In another study, Verma et al. (2018) investigated the effect of CuO-MWCNTs/water and MgO- MWCNTs/waterhybrid nanofluids on thermal and exergetic efficiencies of FPSC. The tests are carried out at different hybrid nanoparticles concentrations ($0.25 - 2.0 vol.\%$) and volume flow rates (0.5 −2.0 L/min). They noticed that the FPSC operates in optimum conditions at concentrations and mass flow rates in the range 0.75–1.0 vol% and 0.025–0.03 kg/s respectively. The results indicated an enhancement in thermal efficiency of 70.55% and 69.11% for MgO-MWCNTs/water and CuO-MWCNTs/water hybrid nanofluids. The exergetic efficiency obtained is 71.54% and 70.63% for the two studied hybrid nanofluids. Sundar et al. (2018) investigated experimentally the efficiency of FPSCs with and without twisted tape inserts using Al_2O_3/water nanofluid. The FPSC is located in Hyderabad, India, and is tested at three mass flow rates (0.033, 0.05, 0.066, 0.083 kg/s) and two nanoparticles concentrations, 0.1 vol% and 0.3 vol% respectively. They observed by adding 0.3 vol% Al_2O_3 nanoparticles in water, the efficiency is enhanced up to 76% for the collector with twisted tape of H/D = 5 and mass flow rate of 0.083 kg/s, compared to the collector without inserts and using water as the working fluid. In another research, Mirzaei et al. (2018) focused on optimal working conditions of the FPSC using 0.1 wt% Al_2O_3dispersed in water. The FPSC is positioned to inclination angle of 45° and is located in Rafsanjan, Iran. The collector is tested in the time interval 10:00 a.m. - 12:00 a.m., for the following flow rates: 1.0, 2.0 and 4 L/min. The results indicated that using a mass concentration of 0.1% Al_2O_3, the thermal efficiency is enhanced by up to 23.6% compared to the base fluid, at a flow rate $of 2L/\min$ which is considered the optimum flow rate. Kiliç et al. (2018) performed an experimental research on the impact of using 2.0 wt% TiO_2/water nanofluid with Triton X-100 as surfactant in an FPSC, located in Ankara, Turkey. They have shown that the nanofluid with the mass flow rate of 0.033 kg/s raises the collector instantaneous efficiency by about 48.67%. A study conducted by Sharafeldin and Gróf (2018) investigated the influence of the concentration of CeO_2 nanoparticles dispersed in water and mass flux rate on the efficiency of FPSC, located in Budapest, Hungary. The tests are performed at concentrations of CeO_2 nanoparticles of 0.0167%, 0.0333% and 0.0666 vol%, and mass flux rates of 0.015, 0.018 and 0.019 kg/s•m^2. The results showed that the improvement in thermal efficiency is 10.74% at a concentration of 0.066 vol% and a mass flux rate of 0.019 kg/s•m^2. Tong et al. (2019) investigated the thermal and exergetic efficiencies of the FPSC using Al_2O_3/water and CuO/water nanofluids, located in Gwangju, Korea. The tests are conducted between 10:00 a.m. and 5:00 p.m. for a mass flow rate of 0.047 kg/s and three concentrations, 0.5, 1.0 and 1.5 vol%. The results revealed that 1.0 vol% Al_2O_3/water nanofluid exhibits the higher thermal and exergetic efficiencies compared to CuO/water nanofluid and water. Elshazly et al. (2022) studied experimentally the thermal and exergetic efficiencies of FPSC using MWCNT, Al_2O_3 and MWCNT-Al_2O_3 (50:50%) nanoparticles dispersed in water. The results indicated that the maximum improvement in thermal and exergetic efficiency is obtained for MWCNT/water nanofluid.

According to the state of the art of above-mentioned articles, there is an increasing trend to use nanofluids in the FPSC. Most studies investigate water – based nanofluids. Studies on performance of FPSC using ionic liquids or ethylene glycol are very limited. In this context, the main goal of the current paper is to investigate the effects of advanced heat transfer fluids including ionanofluids ($[B_{mim}]BF_4$ + GE, $[B_{mim}]BF_4$+SWCNTs and $[C_{4mim}]NTf_2$+Al_2O_3) and nanofluids (water-+Al_2O_3 and ethylene glycol+Al_2O_3) with different concentrations on the performance of a FPSC using a theoretical model. Also, this study uses experimental data for thermo-physical properties of working fluids in calculation of FPSC efficiency and FOM's. The results of this paper emphasize that working fluid can be used for a high performance of the collector under real weather conditions.

Table 1
Specifications of the FPSC (Verma et al., 2017).

Specifications	*Dimensions*
Area of collector,	750x500x63 mm^2
Absorption area of collector	0.375m^2
Absorbing plate emissivity	0.12
Absorptance-transmittance product	0.816
Edge area of collector	0.1572m^2
Glass emissivity	0.88
Glazing plate number	1
Inner diameter of tube	8mm
Outer diameter of tube	10mm
Thermal conductivity of back insulation	0.04W/(m • K)
Thermal conductivity of absorbing plate	390W/(m • K)
Thickness of glazing	4mm
Thickness of back insulation	50mm

2. Empirical correlations for the FPSC efficiency

In the current study, a FPSC with the specifications given in Table 1 is considered. The analysis is based on real weather data for August in Brasov, Romania. Table 2 depicts the average values of solar intensity, outside temperature, and wind velocity for August in Brasov, Romania.

The instantaneous efficiency, defined as the ratio between the energy actually absorbed and transferred to the working fluid and the total input solar energy can be written as:

$$\eta = \frac{Q_u}{A_c \bullet G_t} = F_R \bullet \left[(\tau \bullet \alpha)_e - \frac{U_L \bullet (T_{f,in} - T_a)}{A_c \bullet G_t} \right] \tag{1}$$

and

$$\eta = F_R \bullet \left[k_\theta \bullet (\tau \bullet \alpha)_e - \frac{U_L \bullet \left(T_{f,in} - T_a\right)}{A_c \bullet G_t} \right] \tag{2}$$

The Eq. (1) is valid for a collector angle of $\theta = 90°$, and the Eq. (2) for $\theta < 90°$ respectively. The useful energy, Q_u, is (Duffie snd Beckman, 2013):

$$Q_u = A_c \bullet F_R \bullet \left[G_t \bullet (\tau \bullet \alpha)_e - U_L \bullet \left(T_{f,in} - T_a\right) \right] \tag{3}$$

The collector heat removal factor, F_R, is the ratio of the actual useful energy gain and the heat transfer rate at which the temperature difference between the absorber and environment is minimum. The factor, F_R, can be expressed as:

$$F_R = \frac{\dot{m} \bullet c_p}{U_L \bullet A_c} \bullet \left[1 - \exp\left(- \frac{F^{'} \bullet U_L \bullet A_c}{\dot{m} \bullet c_p} \right) \right] \tag{4}$$

The incident angle modifier is $k_\theta = 1 - b_0 \left(\frac{1}{\cos\beta} - 1 \right)$ (Duffie snd Beckman, 2013). For a single glass collector, the incidence angle modifier coefficient is $b_0 = 0.1$.

The product of transmittance absorptance is about 1% greater than the product of τ and α (Duffie snd Beckman, 2013):

$$(\tau \bullet \alpha)_e \cong 1.02 \bullet (\tau \bullet \alpha) \tag{5}$$

The overall heat loss coefficient, U_L, takes into account the top, bottom and edge loss coefficients, thus (Kalogirou, 2013):

$$U_L = U_t + U_b + U_e \tag{6}$$

where:

The top loss coefficient is given by Klein correlation (Klein, 1975):

$$U_t = \left[\frac{N_g}{\left(\frac{C}{T_{pm}} \right) \bullet \left(\frac{T_{pm} - T_a}{N_g + f} \right)^{0.33}} + \frac{1}{h_w} \right]^{-1} + \left[\frac{\sigma \bullet \left(T_{pm}^2 + T_a^2 \right) \bullet \left(T_{pm} + T_a \right)}{\frac{1}{\varepsilon_p + 0.05 \bullet N_g \bullet \left(1 - \varepsilon_p\right)} + \frac{\left(2 \bullet N_g + f - 1\right)}{\varepsilon_g} - N_g} \right] \tag{7}$$

where:

$$C = 365.9 \bullet \left(1 - 0.00883 \bullet \beta + 0.0001298 \bullet \beta^2\right)$$

$$f = \left(1 - 0.04 \bullet h_w + 0.0005 \bullet h_w^2\right) \left(1 + 0.091 \bullet N_p\right)$$

Table 2
Meteorological data for August in Brasov.

Time	Solar intensity [W/m²]	Outside temperature [℃]	Wind velocity [m/s]
08:45	393	16.21	2
09:45	565	17.29	
10:45	687	18.37	
11:45	737	19.24	
12:45	729	19.87	

$$h_w = \left(8.6 \bullet v_w^{0.6}\right) / L^{0.4}$$

The mean plate temperature, T_{pm}, is computed as follows:

$$T_{pm} = T_{f,in} + \frac{Q_u}{A_c \bullet F_R \bullet U_L} (1 - F_R) \tag{8}$$

Because for determination of the mean plate temperature, T_{pm}, it is necessary to know the quantities of Q_u, U_L and F_R, that depends of T_{pm}, in the first stage T_{pm} is estimated. With this value, Q_u, U_L and F_R are computed. In the second stage, with the obtained values for Q_u, U_L and F_R, the plate the temperature T_{pm} is calculated using Eq. (8). This iterative process is repeated until the results are sufficiently accurate:

$$\left[\frac{\left(T_{pm}\right)_{estimated} - \left(T_{pm}\right)_{calculated}}{\left(T_{pm}\right)_{calculated}} \right] \bullet 100 \leq 10^{-5} \tag{9}$$

The bottom loss coefficient is given by:

$$U_b = \frac{1}{\frac{t_b}{k_b} + \frac{1}{h_{b,a}}} \tag{10}$$

The edge loss coefficient is expressed as:

$$U_e = \frac{1}{\frac{t_e}{k_e} + \frac{1}{h_{e,a}}} \bullet \frac{A_e}{A_c} \tag{11}$$

The heat transfer coefficients in the bottom and the edges can be assumed as $5 \left[\frac{W}{m^2 \bullet K} \right]$ (Mahian et al., 2014).

The collector efficiency factor, $F^{'}$, is obtained by:

$$F^{'} = \frac{\frac{1}{U_L}}{W \bullet \left[\frac{1}{U_L \bullet [D + (W - D) \bullet F]} + \frac{1}{\pi \bullet D_i \bullet h_{fi}} \right]} \tag{12}$$

The standard fin efficiency, F, can be determined as:

$$F = \frac{\tanh \bullet \left[\frac{m \bullet (W - D)}{2} \right]}{\frac{m \bullet (W - D)}{2}} \tag{13}$$

where $m = \sqrt{\frac{U_L}{k_c \bullet t_c}} \left[\frac{1}{m} \right]$ – parameter.

The internal heat transfer coefficient, h_{fi}, can be obtained by Nusselt number as follows:

$$h_{fi} = \frac{Nu \bullet k_{wf}}{D_i} \tag{14}$$

where k_{wf} is the thermal conductivity of the working fluid.

The Nusselt number in turbulent flow is described by the Gnielinski correlation (Bejan, 2013):

$$Nu = \frac{\left(\frac{f}{8} \right) (\mathrm{Re} - 1000) \mathrm{Pr}}{1 + 12.7 \sqrt{f/8} \left(\mathrm{Pr}^{\frac{2}{3}} - 1 \right)} \tag{15}$$

where: $f = [0.79 \ln(\mathrm{Re}) - 1.64]^{-2}$ - friction factor $\mathrm{Re} = \frac{4 \bullet \dot{m}}{\pi \bullet D_i \bullet \mu_{wf}}$ - Reynolds number $\mathrm{Pr} = \frac{\mu_f \bullet c_{p,wf}}{k_{wf}}$ - Prandtl number.

The Eq. (15) is valid for Reynolds number within the range $3 \bullet 10^3 - 5 \bullet 10^6$.

In laminar flow, the Nusselt number is (Bejan, 2013):

$$Nu = \begin{cases} 1.953 \bullet (x_*)^{-\frac{1}{3}} & for \quad x_* \leq 0.03 \\ 4.364 + \dfrac{0.0722}{x_*} & for \quad x_* > 0.03 \end{cases} \tag{16}$$

where $x_* = \frac{x / D_i}{\mathrm{Re} \bullet \mathrm{Pr}}$.

Based on the theoretical model, a computational routine to

estimation of the FPSC efficiency under Romanian weather conditions was developed in Mathcad software (Fig. 1).

3. Thermo-physical properties of the working fluids

Ionanofluids and nanofluids with several base fluids (ionic liquid, water, water and ethylene glycol) are considered for the study of the FPSC. In order to get valid results, the experimental data concerning thermal conductivity, viscosity, density, and specific heat are extracted from the available literature. The studied working fluids are given in Table 3:

The thermo-physical properties of ionic liquids are taken from Zhang et al. (2016) and Paul et al. (2015) and those for water+Al_2O_3 and ethylene glycol+Al_2O_3 are evaluated using the following correlations based on experimental data (Maiga et al., 2004):

water+Al_2O_3

$$\frac{k_{wf}}{k_{bf(T)}} = 4.97 \bullet \phi^2 + 2.72 \bullet \phi + 1 \tag{17}$$

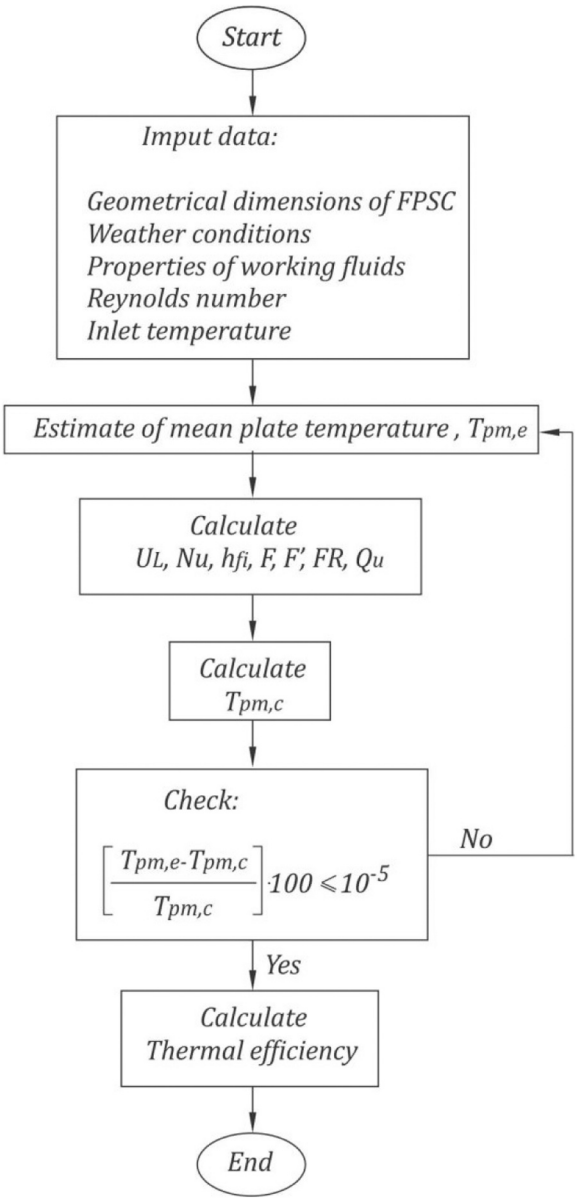

Fig. 1. – Flowchart for calculating FPSC efficiency.

Table 3
Studied working fluids.

Working fluids	Concentration	Reference
$[B_{mim}]BF_4$	0	Zhang et al. (2016)
$[B_{mim}]BF_4$ + GE	0.005 and 0.01 wt%	
$[B_{mim}]BF_4$ + SWCNTs	0.005 and 0.01 wt%	
$[C_{4mim}]NTf_2$	0	Paul et al. (2015)
$[C_{4mim}]NTf_2$ + Al_2O_3	0.18; 0.36 and 0.90 vol%	
Water	0	Incropera et al. (2007)
Water + Al_2O_3	0.18; 0.36 and 0.90 vol%	Maiga et al. (2004)
Ethylene glycol	0	Incropera et al. (2007)
Ethylene glycol + Al_2O_3	0.18; 0.36 and 0.90 vol%	Maiga et al. (2004)

$$\frac{\mu_{wf}}{\mu_{bf(T)}} = 123 \bullet \phi^2 + 7.3 \bullet \phi + 1 \tag{18}$$

ethylene glycol+Al_2O_3

$$\frac{k_{wf}}{k_{bf(T)}} = 28.905 \bullet \phi^2 + 2.8273 \bullet \phi + 1 \tag{19}$$

$$\frac{\mu_{wf}}{\mu_{bf(T)}} = 306 \bullet \phi^2 - 0.19 \bullet \phi + 1 \tag{20}$$

The densities and specific heats of working are computed using the equations for the two-phase mixture:

$$\rho_{wf} = \phi \bullet \rho_{np} + (1 - \phi) \bullet \rho_{bf} \tag{21}$$

$$c_{p,wf} = \frac{\phi \bullet (\rho \bullet c_p)_{np} + (1 - \phi) \bullet (\rho \bullet c_p)_{bf}}{\phi \bullet \rho_{np} + (1 - \phi) \bullet \rho_{bf}} \tag{22}$$

The values of density and the heat specific of Al_2O_3 NPs are 3900kg/m^3 and 880J/(kg • K) respectively (Heyhat et al., 2013).

4. Results and discussion

In order to evaluate of the thermal efficiency of the FPSC located in Brasov, Romania, several working fluids are studied. The analyses are carried out for different types of nanoparticles with various NPs concentrations (0.005 wt% GE, 0.01 wt% GE, 0.005 wt% SWCNTs, 0.01 wt % SWCNTs, 0.18, 0.36 and 0.90 vol% Al_2O_3, adding into $[B_{mim}]$ BF_4 and $[C_{4mim}]$ NTf_2 ionic liquids, water and ethylene glycol. The impact of type of working fluid, concentration of nanoparticles, Reynolds number (100, 200, 300), ambient temperature (16.21; 17.29; 18.28; 19.24; 19.97 ℃) and solar intensity (393, 565, 687, 737, 729 W/m^2) on thermal efficiency are analyzed. The inlet temperature of the working fluids is 20 ℃. The flat-plate solar collector is kept at an inclination angle of 37°.The thermal efficiencies are computed by the average values of outside temperature and solar intensity for August in Brasov.

4.1. Validation of FPSC model with experimental and numerical data

The first stage, the theoretical model for the FPSC using water was validated with the experimental and numerical data from Refs. (Verma et al., 2017, Geovo et al., 2013). The validation was performed in following conditions: the ambient temperature, T = 296.15 K, the mass flow rate, $\dot{m}$ = 0.0167kg/s, and the solar irradiance, G_t = 900W/m^2. The inlet temperature of the water was variable.

The Relative Error (RE) and Mean Relative Error (MRE) were calculated by comparing the current results with numerical and experimental data.

The RE and MRE are computed as:

$$RE = \frac{\sum_{i=1}^{N}\left(\eta_{\exp/num} - \eta_{current\quad results}\right)}{\sum_{i=1}^{N}\eta_{\exp/num}} \bullet 100[\%] \tag{23}$$

$$MRE = \frac{RE}{N} \tag{24}$$

The thermal efficiency of the FPSC as a function of the reduced temperature values $\left[\left(T_{fi} - T_a\right)/G_t\right]$ is shown in Table 4.

As shown in Table 4, the model accurately predicts the experimental and numerical data and can be used to estimation of FPSCs efficiency with various working fluids under Romanian weather conditions.

4.2. Thermal efficiency of FPSC using ionic liquids

In Fig. 2(a-c), the FPSC efficiency is plotted as a function of reduced temperature parameter $(T_{in} - T_a)/G_t$ for $[B_{mim}]$ BF_4 with two different types of nanoparticles, GE and SWCNTs, at different weight concentrations and Reynolds numbers. As seen, the efficiency of $[B_{mim}]$ BF_4 is higher than that of $[B_{mim}]$ BF_4 +GE and $[B_{mim}]$ BF_4 +SWCNTs indifferent of concentration. The efficiency of $[B_{mim}]$ BF_4 +GE has a opposite trend compared to $[B_{mim}]$ BF_4 + SWCNTs. For $[B_{mim}]$ BF_4 + GE, the efficiency decreases with increasing the concentration, while for $[B_{mim}]$ BF_4 + SWCNTs, the efficiency increases with increasing concentration, the concentration, but not exceeding the efficiency of the base fluid. When $[B_{mim}]$ BF_4 +GE is used in FPSC, the mean temperature of the plate increases with the adding of nanoparticles, the useful energy, Q_u is smaller and the efficiency is reduced. In the case of $[B_{mim}]$ BF_4 + SWCNTs, the mean temperature of plate decreases with the adding of nanoparticles, which leads to an increase in both useful energy and efficiency. This behavior could be explained by the fact that the useful energy, Q_u depends on the properties of the working fluids. Thus, the viscosity of $[B_{mim}]$ BF_4 +GE decreases with increasing concentration, while for $[B_{mim}]$ BF_4 + SWCNTs, the viscosity increases with increasing concentration. Another reason for the reduced efficiency of $[B_{mim}]$ BF_4 ionic liquids with nanoparticles can be the relatively low concentration. A higher concentration of SWCNTs could probably lead to a higher efficiency than the base fluid. With an increase in Reynolds number, the mean temperature of the plate is reduced and can be seen as an improvement of the efficiency of FPSC.

Since the studied $[B_{mim}]$ BF_4 ionic liquid with nanoparticles did not emphasize an improvement in FPSC thermal efficiency, and another type of ionic liquid is analyzed. Fig. 3(a-c) depicts the thermal efficiency of FPSC using $[C_{4mim}]$ NTf_2 with different Al_2O_3 concentrations. As can be seen, the addition of nanoparticles in the ionic liquid, in this case, leads to an improvement in the thermal efficiency. The maximum relative increase in thermal efficiency compared to the base fluid is achieved to Re= 100for all studied concentrations. With the increase in Reynolds number, the FPSC efficiency increases, but the presence of nanoparticles in the ionic liquids has a smaller contribution to increasing efficiency. This behavior can be explained by the heat removal factor, F_R, which depends of the solar collector characteristics, the type of working fluid, and the flow rate in collector. Thus, F_R increases with both increasing in the Reynolds number and concentration. At Re= 100 and 0.9 vol% Al_2O_3 NPs, the relative increasing in F_R is 4.71%, while at Re= 300, the increase is 2.79%, for the same concentration.

4.3. Thermal efficiency of FPSC using water

Fig. 4(a-c) illustrates the thermal efficiency of the FPSC using water with Al_2O_3 NPs as the working fluid for different nanoparticles concentrations and Reynolds numbers. Compared to ionic liquids, a significant decrease in FPSC efficiency using water can be observed. However, the adding Al_2O_3 NPs to the water, as well as increasing the Reynolds number leads to a more significant improvement in FPSC efficiency. With the increase of the Reynolds number, the same effect of the concentration on the efficiency of the collector can be observed as in the case of using ionic liquids. Although the influence of nanoparticles is lower with increasing Reynolds number, an increase in efficiency can still be observed compared to the base fluid.

4.4. Thermal efficiency of FPSC using ethylene glycol

The thermal efficiency of the FPSC using ethylene glycol with Al_2O_3 NPs is shown in Fig. 5(a-c). In contrast to the FPSC using water+ Al_2O_3 and $[C_{4mim}]$ NTf_2 +Al_2O_3, from Fig. 5(a-c) it can be seen that the addition of Al_2O_3 NPs to ethylene glycol does not contribute to the improvement in the FPSC efficiency. There is a slowly increase in efficiency, but this is insignificant and cannot justify the use of nanoparticles. An increase in FPSC efficiency can be observed with increasing Reynolds number, its values being close to FPSC efficiency values using $[C_{4mim}]$ NTf_2 ionic liquid.

Fig. 6(a-c) illustrates the effect of solar intensity on the thermal efficiency of FPSC using various working fluids. It is seen that the efficiency increases with increasing solar intensity up to $729 W/m^2$ for all fluids. At a solar intensity of $737 W/m^2$, a slight decrease in thermal efficiency can be observed, that could be explained by the increase the heat loss to the surrounding. Table 5 shows the absorbed energy by the solar collector, $F_R(\tau\alpha)$, and the heat loss to the surrounding, $F_R U_L$ at various Reynolds numbers. The absorbed energy by the solar collector, $F_R(\tau\alpha)$ gradually increases as the Reynolds number increased. Generally, the heat loss values, $F_R U_L$, show the same tendency for all the Reynolds numbers, the increase in flow rate leading to more heat loss to the surrounding. As can be seen, the $F_R(\tau\alpha)$ values for 0.01 wt% GE and 0.01 wt % SWCNTs ionanofluid were lower than using only $[B_{mim}]$ BF_4 for all Reynolds numbers, while the $F_R(\tau\alpha)$ values for 0.9 vol% Al_2O_3 were higher than those for $[C_{4mim}]NTf_2$ and water, except the value of the water+ 0.9 vol% Al_2O_3 nanofluid at Re = 200 and $G_t = 737 W/m^2$. The $F_R(\tau\alpha)$ values for the EG+ 0.9 vol% Al_2O_3 nanofluid were very close to those of EG.

Analyzing Fig. 6 it can be stated that $[C_{4mim}]$ NTf_2 +0.9vol.%Al_2O_3 ionic liquid have the highest thermal efficiency at any Reynolds number and solar intensity, while water+ 0.9 vol% Al_2O_3 nanofluids have the lowest values of efficiency. Moreover, it can be seen that the addition of nanoparticles in the base fluid is only beneficial for $[C_{4mim}]$ NTf_2 ionic liquid and water. For the other studied working fluids, the addition of

Table 4
Comparison of the FPSC efficiency with the experimental (Verma et al., 2017) and numerical data (Geovo et al., 2013).

$(T_{fi} - T_a)/G_t$	η_{exp} Ref. (Verma et al., 2017)	η_{num} Ref. (Geovo et al., 2013)	$\eta_{current\ results}$	*RE* compared to Ref.(Verma et al., 2017)	*RE* compared to Ref. (Geovo et al., 2013)
0.00571	60.26	62.41	61.416	1.918	1.593
0.01023	59.24	60.78	60.224	1.661	0.915
0.01467	57.82	59.14	58.832	1.75	0.521
0.02363	55.30	55.69	56.048	1.353	0.643
0.02808	54.28	53.93	54.503	0.411	1.062
0.03071	53.50	52.87	53.708	0.389	1.585
0.03553	52.16	50.89	51.657	0.964	1.507
MRE (%)				1.207	1.118

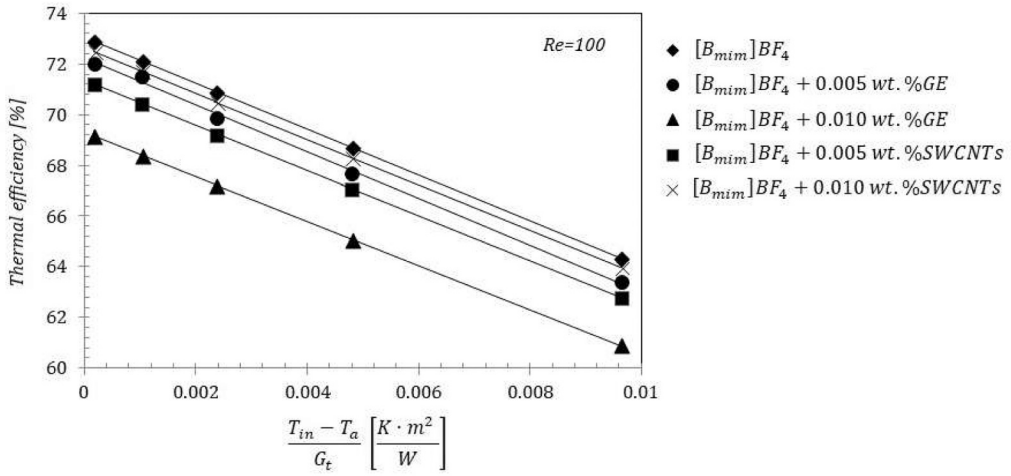

a)

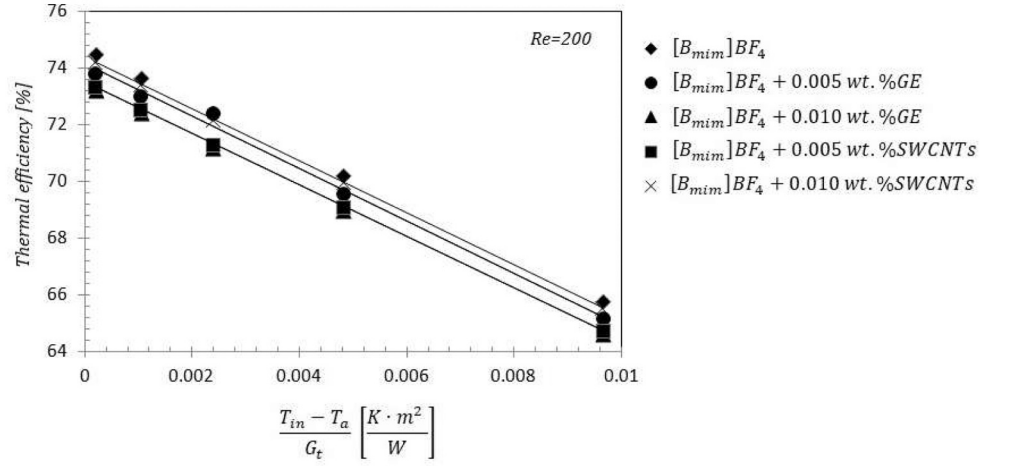

b)

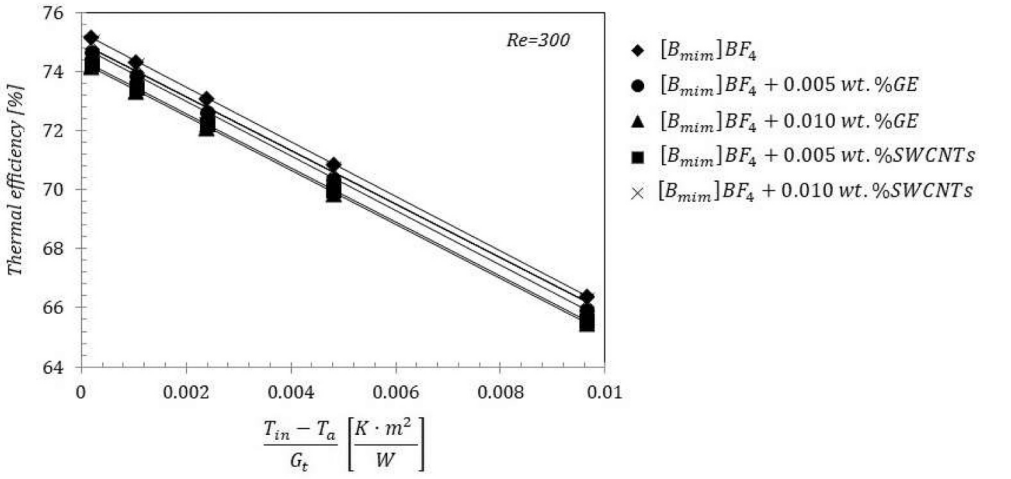

c)

Fig. 2. – Thermal efficiency of $[B_{mim}]$ BF_4 with various NPs at different Reynolds number.

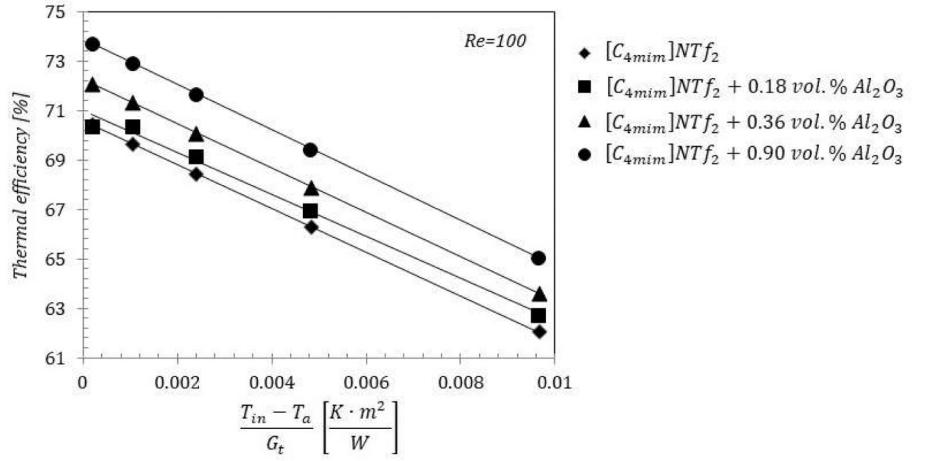

a)

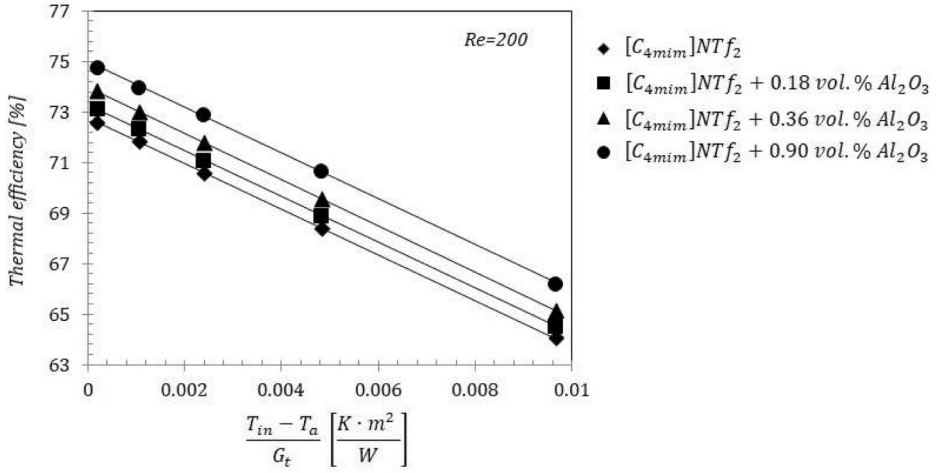

b)

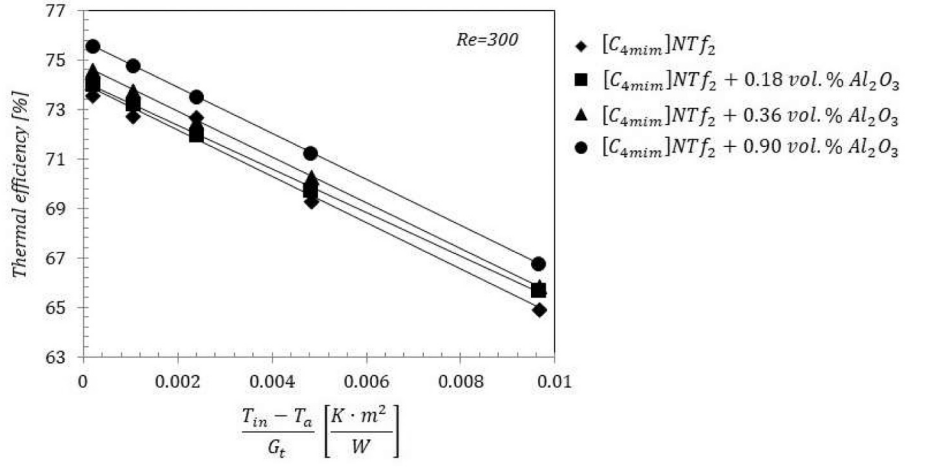

c)

Fig. 3. – Thermal efficiency of $[C_{4mim}]\ NTf_2$ with Al_2O_3 NPs at different Reynolds number.

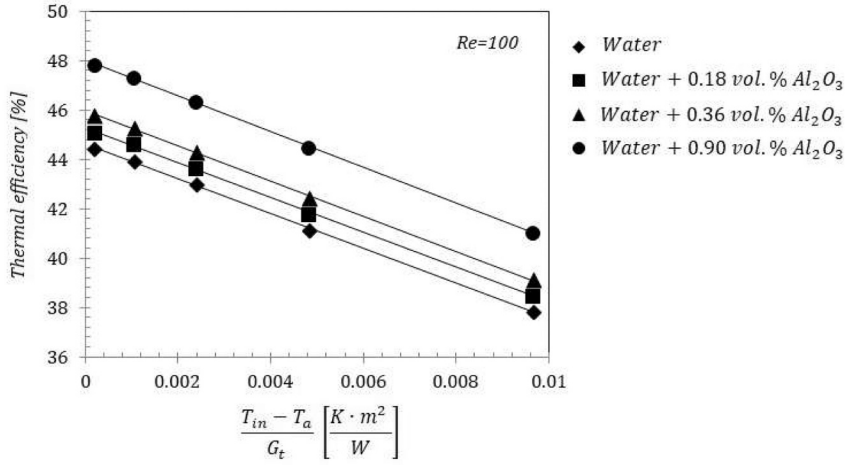

a)

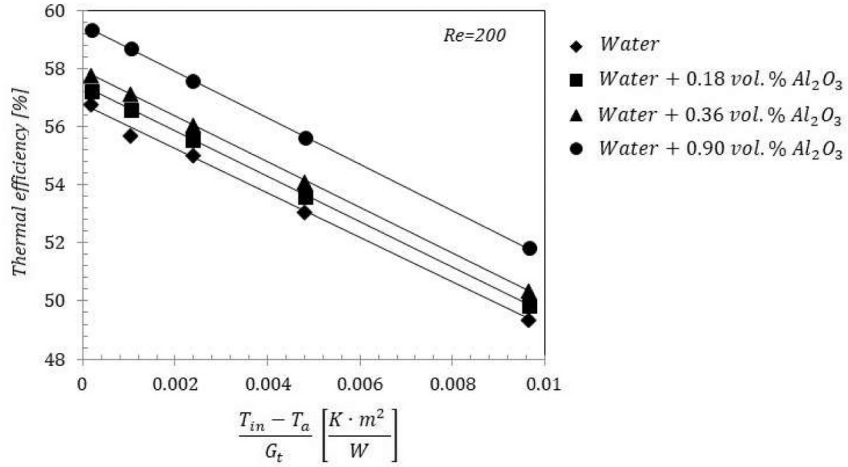

b)

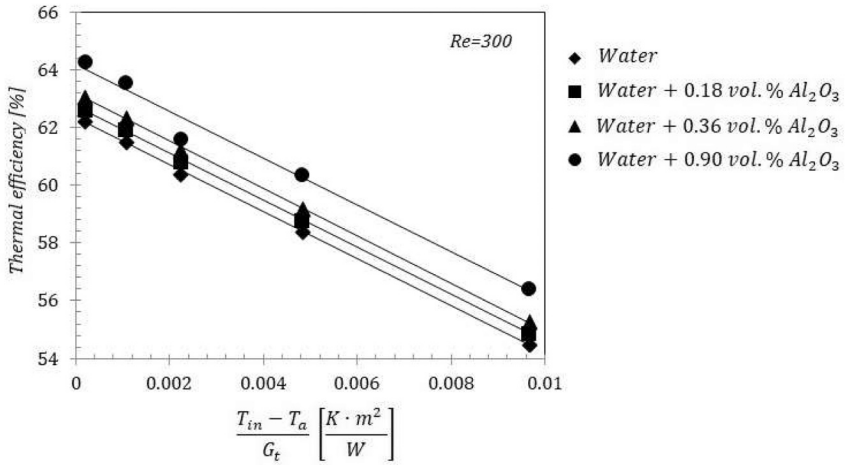

c)

Fig. 4. – Thermal efficiency of water with Al_2O_3 NPs s at different Reynolds number.

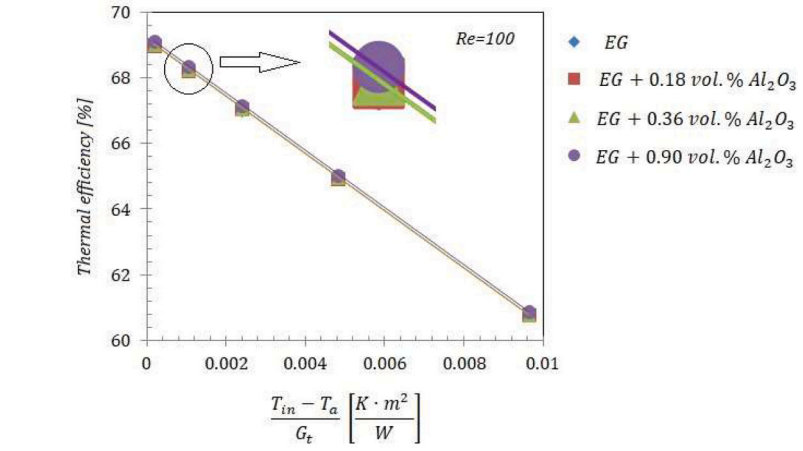

a)

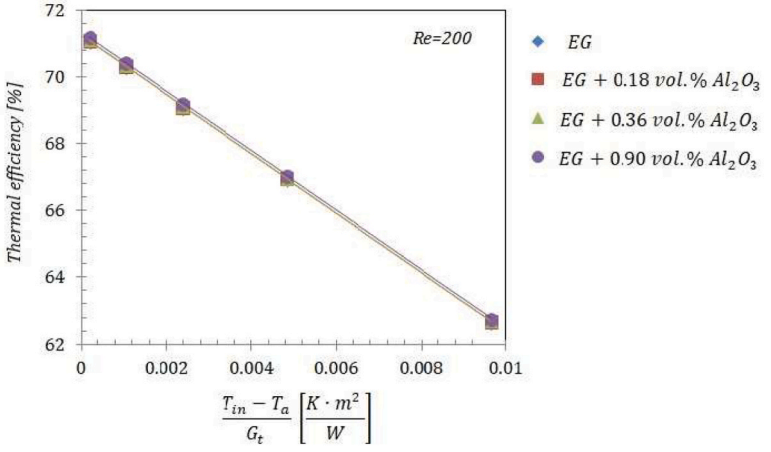

b)

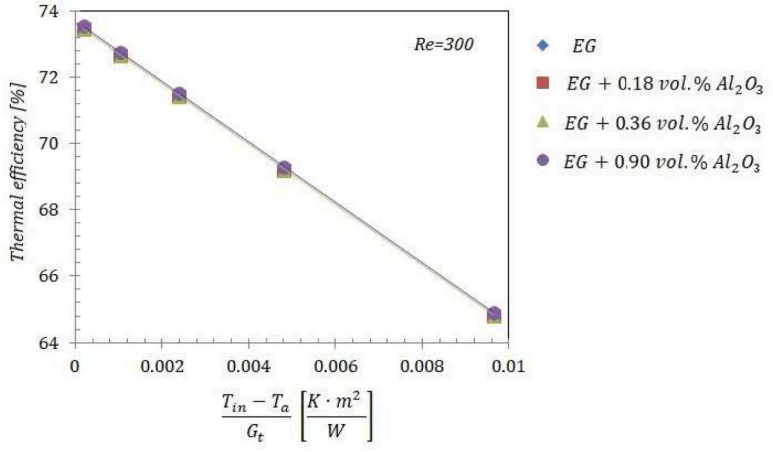

c)

Fig. 5. – Thermal efficiency of ethylene glycol with Al_2O_3 NPs at different Reynolds number.

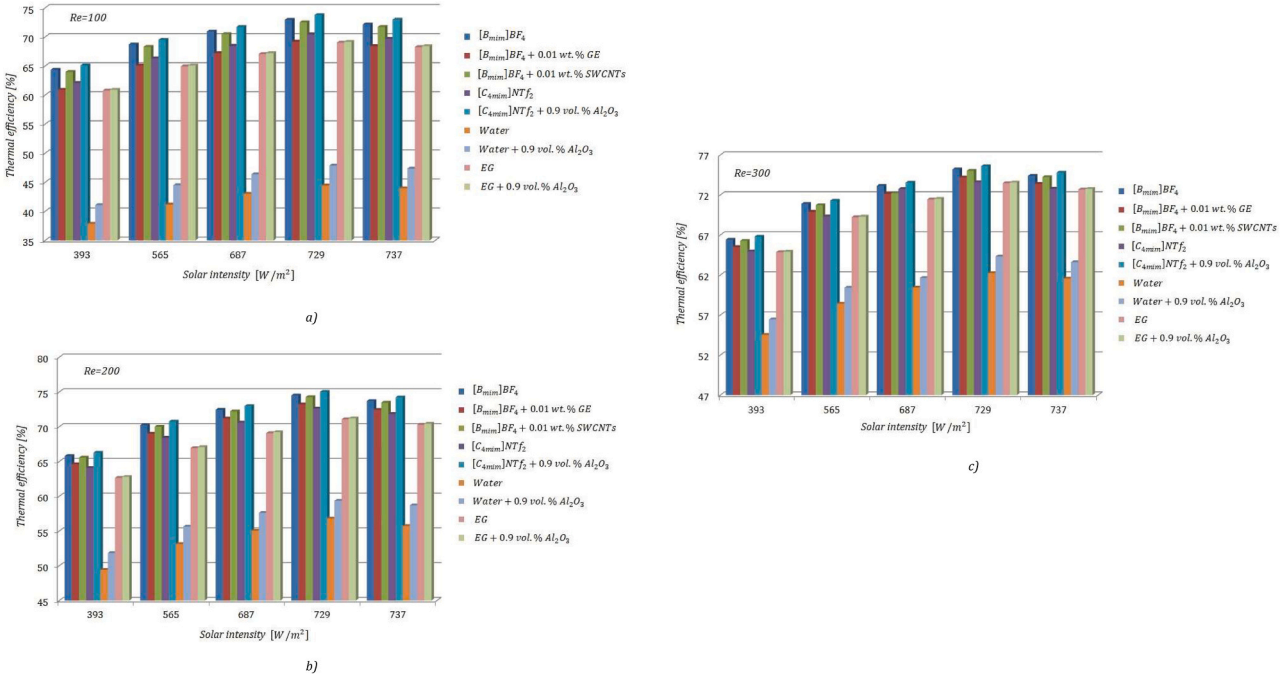

Fig. 6. – Thermal efficiency as a function of solar intensity.

Table 5
. F_RU_L and $F_R(\tau\alpha)$ for all working fluids.

Reynolds number	100				200				300			
Solar Intensity	729		737		729		737		729		737	
Parameters	F_RU_L	$F_R(\tau\alpha)$	F_RU_L	$F_R(\tau\alpha)$	F_RU_L	$F_R(\tau\alpha)$	F_RU_L	$F_R(\tau\alpha)$	F_RU_L	$F_R(\tau\alpha)$	F_RU_L	$F_R(\tau\alpha)$
$[B_{mim}]$ BF_4	8.431	0.754	8.549	0.753	8.472	0.77	8.633	0.769	8.457	0.777	8.646	0.776
$[B_{mim}]BF_4$ + 0.01wt.%GE	8.292	0.733	8.378	0.733	8.444	0.757	8.569	0.756	8.471	0.767	8.621	0.766
$[B_{mim}]BF_4$ + 0.01wt.% SWCNTs	8.407	0.75	8.518	0.749	8.472	0.768	8.625	0.767	8.463	0.775	8.645	0.775
$[C_{4mim}]$ NTf_2	8.247	0.728	8.327	0.727	8.414	0.751	8.526	0.750	8.458	0.761	8.592	0.760
$[C_{4mim}]$ NTf_2 + 0.9vol.% Al_2O_3	8.463	0.762	8.601	0.762	8.463	0.775	8.645	0.775	8.434	0.781	8.644	0.781
Water	4.924	0.459	4.931	0.459	6.539	0.587	4.816	0.652	7.282	0.643	7.314	0.643
Water+ + 0.9vol.% Al_2O_3	5.37	0.495	5.379	0.494	6.9	0.614	6.925	0.613	7.549	0.665	7.589	0.664
EG	8.104	0.713	8.171	0.713	8.302	0.735	8.39	0.737	8.454	0.76	8.585	0.759
EG+ + 0.9vol.% Al_2O_3	8.119	0.715	8.187	0.714	8.314	0.736	8.404	0.735	8.457	0.76	8.589	0.759

nanoparticles reduces or does not influence the efficiency of the collector. However, it can be concluded that the ionic liquids and ethylene glycol are beneficial in flat plat solar collectors, because they ensure a higher efficiency compared to water.

4.5. Comparison of the FPSC thermal efficiency with various FOMs

In this study, the numbers of figure-of-merits (FOMs) are considered for comparison of the FPSC efficiency. A first FOM considers the ratio between the relative increases in viscosity against the relative increase in thermal conductivity and is defined as:

$$\frac{C_\mu}{C_k} = \frac{(\mu_{wf} - \mu_{bf})/\mu_{bf}}{(k_{wf} - k_{bf})/k_{bf}} < 4 \tag{25}$$

Fig. 7 depicts a comparison of C_μ/C_k values for the studied working fluids. It can be seen that, the working fluids based on water, ethylene glycol and $[C_{4mim}]$ NTf_2 ionic liquid, excepting $[C_{4mim}]$ NTf_2 + 0.9vol.%Al_2O_3, have ratios lower than 4, which means that they are advantageous for to be used in FPSC. Moreover, it can be noticed that the $[B_{mim}]$ BF_4 ionic liquid with nanoparticles recorded negative values of ratio C_μ/C_k. This is due to their reduced viscosity compared to the base fluid. Comparing to the FPSC efficiency, it can be concluded that, the C_μ/C_k ratio provided results quite close and could be used as merit criterion to establishment the effectiveness of the working fluid.

Another merit criterion investigated is Mouromtseff number (Mo), defined as $Mo = k_{wf}/k_{bf} > 1$. If only the thermal conductivity is taken in the evaluation of the efficiency of the working fluids, then it can be observed from Fig. 8 that all studied fluids have values of the Mo ratio higher than 1. This criterion provides results comparable to those found for FPSC efficiency, excepting the working fluids based on $[B_{mim}]$ BF_4 ionic liquid.

Performance evolution criterion ($PEC_{wf}/PEC_{bf} > 1$), defined as the ratio between the transferred heat and the pumping power, $PEC = \dot{m} \bullet c_p \bullet (T_{out} - T_{in})/(\dot{V} \bullet \Delta p)$, is shown in Fig. 9. It is seen that PEC ratio has higher values than 1 for the working fluids based on $[B_{mim}]$ BF_4 ionic liquid, and lower values than 1 for the other working fluids. These results are in opposite with FPSC efficiency results. The achieved results for the working fluids based on $[B_{mim}]$ BF_4 ionic liquid can be explained by the fact that their viscosities are lower than those of the base fluid, the pressure losses are lower and consequently, the required pumping power is reduced compared to the base fluid. For the other working fluids, the viscosities are higher than those of the base fluid, which means that the pressure losses are higher and implicitly the required pumping power is higher, thus leading to PEC ratios lower than

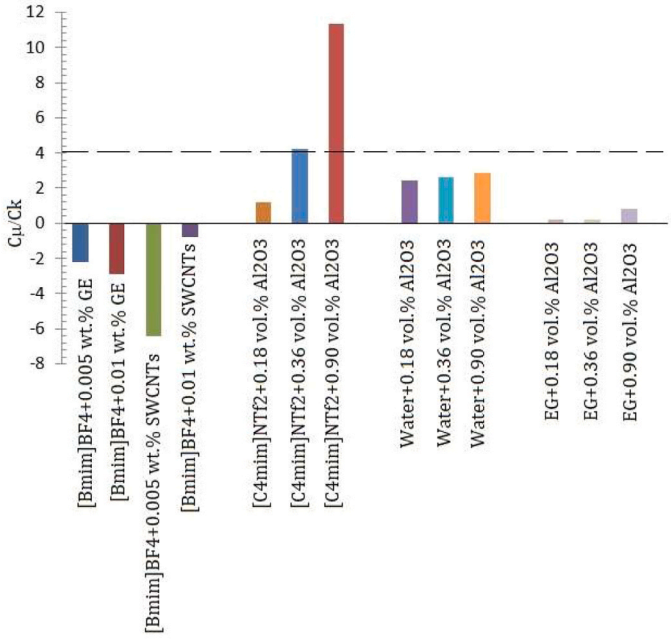

Fig. 7. – C_μ/C_k ratio of studied working fluids.

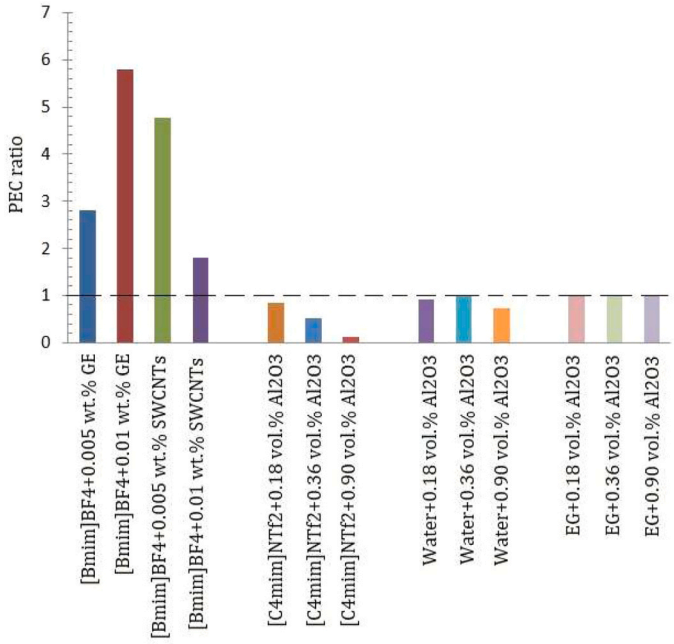

Fig. 9. – PEC ratio at Re= 300 and $G_t = 737 W/m^2$.

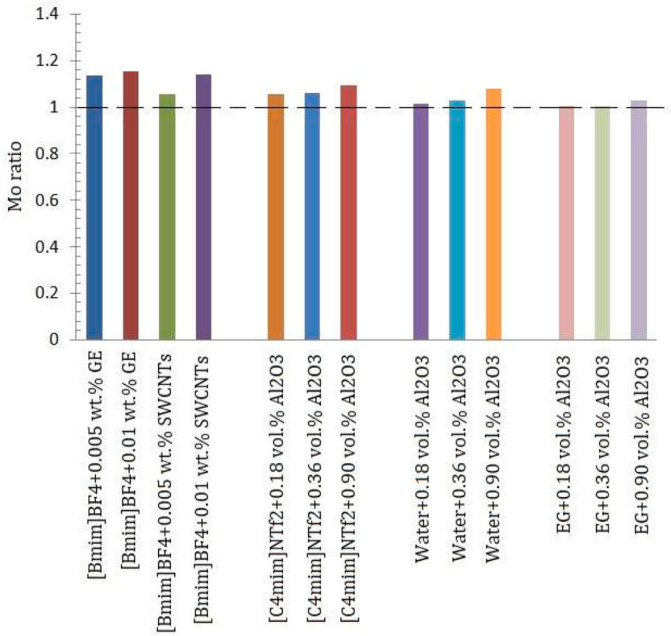

Fig. 8. – Mo ratio of studied working fluids.

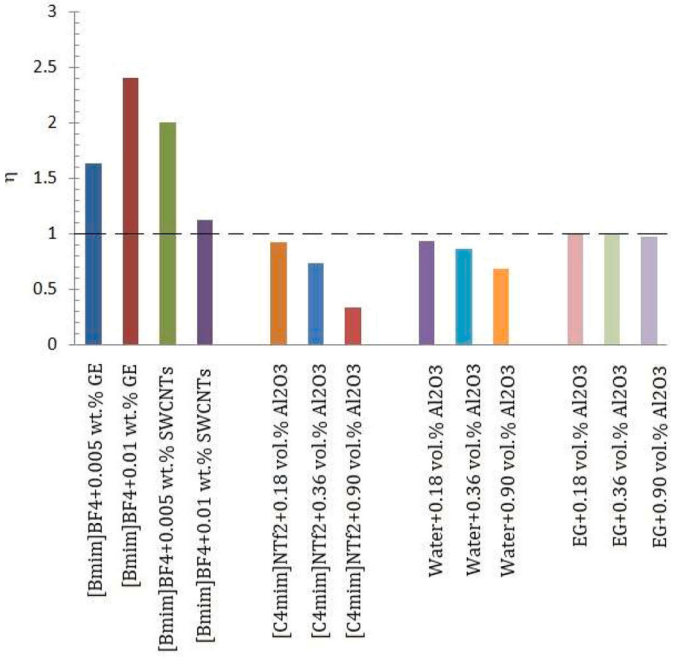

Fig. 10. - Overall energetic efficiency at Re= 300 and $G_t = 737 W/m^2$.

1.

Fig. 10 compares the values of overall energetic efficiency ($\eta_{wf}/\eta_{bf} > 1$), defined as $\eta = (Nu_{wf} \bullet \Delta p_{bf})/(Nu_{bf} \bullet \Delta p_{wf})$. This criterion takes into account the Nusselt number and pressure drop. The results illustrated in Fig. 9 exhibit the same trend with PEC criteria. Although the heat transfer is improved by adding nanoparticles, the increase in pressure drop due to the increase in viscosity is more significant. This leads to lower values than 1 for the overall energetic efficiency, excepting the working fluids based on $[B_{mim}]$ BF_4 ionic liquid.

5. Conclusions

The current study provides a comparative study on the performance of flat-plate solar collectors using several working fluids in real weather conditions. The studied advanced heat transfer fluids have as base fluid: $[B_{mim}]$ BF_4 and $[C_{4mim}]$ NTf_2 ionic liquids, water and ethylene glycol. The study is carried out for different values of solar intensity, Reynolds number, and nanoparticles concentrations. The findings of this study are summarized below:

1. Thermal efficiency depends on the base fluid, the type of nanoparticle, and varies with the nanoparticle concentration. Thus, the efficiency of $[B_{mim}]$ BF_4 ionic liquid is higher than that of $[B_{mim}]$ BF_4 +GE and $[B_{mim}]$ BF_4 + SWCNTs. Adding GE and SWCNTs to the base fluid does not improve FPSC efficiency. In contrast, $[C_{4mim}]$

NTf_2 ionic liquid with different Al_2O_3 concentrations in the FPSC enhances the thermal efficiency. The addition of Al_2O_3 NPs to water leads to a significant improvement in FPSC efficiency, while the addition of Al_2O_3 NPs to ethylene glycol does not contribute to the improvement in the FPSC efficiency.

2. The FPSC efficiency increases with increasing solar intensity for all fluids. $[C_{4mim}]$ NTf_2 +0.9vol.%Al_2O_3 ionic liquid have the highest thermal efficiency at any Reynolds number and solar intensity, while water+ 0.9 vol% Al_2O_3 nanofluids have the lowest values of efficiency.
3. $[C_{4mim}]$ NTf_2 +0.9vol.%Al_2O_3 exhibit $C_\mu/C_k > 4$. This result is not in agreement with the FPSC efficiency. Except for this ionanofluid, all working fluids exhibit $C_\mu/C_k < 4$.
4. All studied fluids have values of Mo > 1. These results are in agreement with the FPSC efficiency, except the$[B_{mim}]$ BF_4 ionic liquid for which the addition of solid particles does not improve the collector efficiency.

P_{wf}/P_{bf} and η_{wf}/η_{bf} criteria have similar trend. $P_{wf}/P_{bf} > 1$ and $\eta_{wf}/\eta_{bf} > 1$ for the working fluids based on $[B_{mim}]$ BF_4 ionic liquid and < 1 for other working fluids. These results are in opposite to FPSC efficiency results.

Following the analysis carried out in this paper, it can be emphasized that the ionic liquids are a good alternative to conventional fluids (e.g. water) to be used in solar collectors for Romanian weather conditions.

CRediT authorship contribution statement

Huminic Angel: Conceptualization, Investigation, Methodology, Validation, Writing – original draft. **Huminic Gabriela:** Conceptualization, Funding acquisition, Investigation, Methodology, Supervision, Validation, Writing – original draft, Writing – review & editing.

Declaration of Competing Interest

The authors declare that they have no known competing financial interests or personal relationships that could have appeared to influence the work reported in this paper.

Data Availability

Data will be made available on request.

Acknowledgments

This work was supported by grants from the Ministry of Education and Research, Romania, CNCS-UEFISCDI, project number PN-III-P4-IDPCE-2020-0353.

References

Ashour, A.F., El-Awady, A.T., Tawfik, M.A., 2022. Numerical investigation on the thermal performance of a flat plate solar collector using ZnO & CuO water nanofluids under Egyptian weathering conditions. Energy J. 240, 122743 https://doi.org/10.1016/j.energy.2021.122743.

Balaji, K., Kumar, P.G., Sakthivadivel, D., Vigneswaran, V.S., Iniyan, S., 2019. Experimental investigation on flat plate solar collector using frictionally engaged thermal performance enhancer in the absorber tube. Renew. Energy 142, 62–72. https://doi.org/10.1016/j.renene.2019.04.078.

Bejan A., 2013. Convection heat transfer, 4th Edition, John Wiley & Sons, Inc., Hoboken, New Jersey. doi:⟨10.1002/9781118671627⟩.

Carmona, M., Palacio, M., 2019. Thermal modelling of a flat plate solar collector with latent heat storage validated with experimental data in outdoor conditions. J. Sol. Energy 177, 620–633. https://doi.org/10.1016/j.solener.2018.11.056.

Duffie J.A., Beckman W.A., 2013. Solar Engineering of Thermal Processes, 4th Edition, John Wiley & Sons. doi:⟨10.1002/9781118671603⟩.

Elcioglu, E.B., Genc, A.M., Karadeniz, Z.H., Ezan, M.A., Turgut, A., 2020. Nanofluid figure-of-merits to assess thermal efficiency of a flat plate solar collector. Energy Convers. Manag. 204, 112292 https://doi.org/10.1016/j.enconman.2019.112292.

Elshazly, E., Abdel-Rehim, A.A., El-Mahallawi, I., 2022. 4E study of experimental thermal performance enhancement of flat plate solar collectors using MWCNT, Al_2O_3, and hybrid MWCNT/ Al_2O_3 nanofluids. Results Eng. 16, 100723 https://doi.org/10.1016/j.rineng.2022.100723.

Fan, M., You, S., Gao, X., Zhang, H., Li, B., Zheng, W., Sun, L., Zhou, T., 2019. A comparative study on the performance of liquid flat-plate solar collector with a new V-corrugated absorber. Energy Convers. Manag 184, 235–248. https://doi.org/10.1016/j.enconman.2019.01.044.

García, A., Herrero-Martin, R., Solano, J.P., Pérez-García, J., 2018. The role of insert devices on enhancing heat transfer in a flat-plate solar water collector. Appl. Therm. Eng. 132, 479–489. https://doi.org/10.1016/j.applthermaleng.2017.12.090.

Geovo, L., Ri, G.D., Kumar, R., Verma, S.K., Roberts, J.J., Mendiburu, A.Z., 2023. Theoretical model for flat plate solar collectors operating with nanofluids: Case study for Porto Alegre, Brazil. Energy J. 263, 125698 https://doi.org/10.1016/j.energy.2022.125698.

He, Q., Zeng, S., Wang, S., 2015. Experimental investigation on the efficiency of flat-plate solar collectors with nanofluids. Appl. Therm. Eng. 88, 165–171. https://doi.org/10.1016/j.applthermaleng.2014.09.053.

Heyhat, M.M., Kowsary, F., Rashidi, A.M., Momenpour, M.H., Amrollahi, A., 2013. Experimental investigation of laminar convective heat transfer and pressure drop of water-based Al_2O_3 nanofluids in fully developed flow regime. Exp. Therm. Fluid Sci. 44, 483–489. https://doi.org/10.1016/j.expthermflusci.2012.08.009.

Incropera F.P., Dewitt D.P., Bergman Tl, Lavine A.S., 2007. Fundamentals of Heat and Mass Transfer, 6th Edition, John Wiley & Sons.

Kalogirou S.A., 2013. Solar energy engineering: processes and systems, 2nd Edition. Oxford: Elsevier.

Kiliç, F., Menlik, T., Sözen, A., 2018. Effect of titanium dioxide/water nanofluid use on thermal performance of the flat plate solar collector. J. Sol. Energy 164, 101–108. https://doi.org/10.1016/j.solener.2018.02.002.

Klein, S.A., 1975. Calculation of fiat-plate collector loss coefficients. J. Sol. Energy 17, 79–80. https://doi.org/10.1016/0038-092X(75)90020-1.

Liu, S., Afan, H.A., Aldlemy, M.S., Al-Ansari, N., Yaseen, Z.M., 2020. Energy analysis using carbon and metallic oxides-based nanomaterials inside a solar collector. Energy Rep. 6, 1373–1381. https://doi.org/10.1016/j.egyr.2020.05.015.

Mahian, O., Kianifar, A., Sahin, A.Z., Wongwises, S., 2014. Performance analysis of a minichannel-based solar collector using different nanofluids. Energy Convers. Manag 88, 129–138. https://doi.org/10.1016/j.enconman.2014.08.021.

Maiga, S.E.B., Nguyen, C.T., Galanis, N., Roy, G., 2004. Heat transfer behaviours of nanofluids in a uniformly heated tube. Superlattices Micro 35, 543–557. https://doi.org/10.1016/j.spmi.2003.09.012.

Mirzaei, M., Hosseini, S.M.S., Kashkooli, A.M.M., 2018. Assessment of Al_2O_3 nanoparticles for the optimal operation of the flat plate solar collector. Appl. Therm. Eng. 134, 68–77. https://doi.org/10.1016/j.applthermaleng.2018.01.104.

Paul, T.C., Morshed, A.K.M., Fox, E.B., Khan, J.A., 2015. Thermal performance of Al_2O_3 nanoparticle enhanced ionic liquids (NEILs) for concentrated solar power (CSP) applications. Int. J. Heat. Mass Transf. 85, 585–594. https://doi.org/10.1016/j.ijheatmasstransfer.2015.01.071.

Said, Z., Saidur, R., Rahim, N.A., 2016. Energy and exergy analysis of a flat plate solar collector using different sizes of aluminium oxide based nanofluid. J. Clean. Prod. 133, 518–530. https://doi.org/10.1016/j.jclepro.2016.05.178.

Said, Z., Saidur, R., Sabiha, M.A., Rahim, N.A., Anisur, M.R., 2015a. Thermophysical properties of single wall carbon nanotubes and its effect on exergy efficiency of a flat plate solar collector. J. Sol. Energy 115, 757–769. https://doi.org/10.1016/j.solener.2015.02.037.

Said, Z., Sabiha, M.A., Saidur, R., Hepbasli, A., Rahim, N.A., Mekhilef, S., Ward, T.A., 2015b. Performance enhancement of a Flat Plate Solar collector using Titanium dioxide nanofluid and Polyethylene Glycol dispersant. J. Clean. Prod. 92, 343–353. https://doi.org/10.1016/j.jclepro.2015.01.007.

Sharafeldin, M.A., Gróf, G., 2018. Experimental investigation of flat plate solar collector using CeO_2-water nanofluid. Energy Convers. Manag. 155, 32–41. https://doi.org/10.1016/j.enconman.2017.10.070.

Sharafeldin, M.A., Grof, G., Mahian, O., 2017. Experimental study on the performance of a flat-plate collector using WO3/Water nanofluids. Energy J. 141, 2436–2444. https://doi.org/10.1016/j.energy.2017.11.068.

Sint, N.K.C., Choudhury, I.A., Masjuki, H.H., Aoyama, H., 2017. Theoretical analysis to determine the efficiency of a CuO-water nanofluid based-flat plate solar collector for domestic solar water heating system in Myanmar. J. Sol. Energy 155, 608–619. https://doi.org/10.1016/j.solener.2017.06.055.

Sundar, L.S., Singh, M.K., Punnaiah, V., Sousa, A.C.M., 2018. Experimental investigation of Al_2O_3/water nanofluids on the effectiveness of solar flat-plate collectors with and without twisted tape inserts. Renew. Energy 119, 820–833. https://doi.org/10.1016/j.renene.2017.10.056.

Tong, Y., Lee, H., Kang, W., Cho, H., 2019. Energy and exergy comparison of a flat-plate solar collector using water, Al_2O_3 nanofluid, and CuO nanofluid. Appl. Therm. Eng. 159, 113959 https://doi.org/10.1016/j.applthermaleng.2019.113959.

Twidell J., Weir T., 2006. Renewable Energy Resources, 2nd edition, Taylor & Francis e-Library. doi.org/10.4324/9780203478721.

Verma, S.K., Tiwari, A.K., Chauhan, D.S., 2017. Experimental evaluation of flat plate solar collector using nanofluids. Energy Convers. Manag 134, 103–115. https://doi.org/10.1016/j.enconman.2016.12.037.

Verma, S.K., Tiwari, A.K., Tiwari, S., Chauhan, D.S., 2018. Performance analysis of hybrid nanofluids in flat plate solar collector as an advanced working fluid. J. Sol. Energy 167, 231–241. https://doi.org/10.1016/j.solener.2018.04.017.

Xu, L., Khalifeh, A., Khandakar, A., Vaferi, B., 2022. Numerical investigating the effect of Al2O3-water nanofluids on the thermal efficiency of flat plate solar collectors. Energy Rep. 8, 6530–6542. https://doi.org/10.1016/j.egyr.2022.05.012.

Zhang, L., Chen, L., Liu, J., Fang, X., Zhang, Z., 2016. Effect of morphology of carbon nanomaterials on thermo-physical characteristics, optical properties and photo-thermal conversion performance of nanofluids. Renew. Energy 99, 888–897. https://doi.org/10.1016/j.renene.2016.07.073.